

Kinetics of discontinuous precipitation and type I discontinuous coarsening in Zn–4 at % Ag alloy

I. MANNA, J. N. JHA, S. K. PABI

Metallurgical and Materials Engineering Department, Indian Institute of Technology, Kharagpur, W. B. 721 302, India

E-mail: bonny@hijli.iitkgp.ernet.in

A detailed study of the kinetics of discontinuous precipitation (DP) and type I discontinuous coarsening (DCI) in Zn–4 at % Ag alloy is reported here for the first time. DCI succeeds DP during prolonged isothermal ageing. Both DP and DCI are characterized by a predominantly lamellar morphology of the precipitate phase, statistically constant interlamellar spacing and steady state reaction front (RF) velocity at a given temperature. The interlamellar spacing increases with temperature. The RF velocity shows a C-curve behavior for DP, but increases monotonically for DCI, as a function of temperature. DCI is distinguished from DP by a 3–5 times larger interlamellar spacing and 1–2 orders of magnitude lower RF velocity than those of DP under comparable conditions. DCI may be initiated from an interface between two DP colonies, a former DP-RF, or the free surface intersecting a DP colony. Kinetic analysis of DP using the models of Turnbull, Cahn, Hillert, and Petermann and Hornbogen, and of DCI using the modified Petermann and Hornbogen model (by Fournelle) have yielded grain boundary diffusivity data in the temperature range 353–573 K. Subsequent Arrhenius analysis shows that the activation energy of the DP and DCI processes lies between 50–66 kJ mol⁻¹. The latter is comparable with the activation energy of grain-boundary self-diffusion of Zn and is nearly half that of tracer impurity diffusion (volume/bulk) of Ag in Zn. Hence, it is concluded that DP and DCI are grain-boundary diffusion-controlled processes in the present alloy. © 1999 Kluwer Academic Publishers

1. Introduction

Formation of a two-phase aggregate comprising a solute-depleted matrix (α) and precipitate phase (β) behind a migrating boundary advancing into a supersaturated solid solution (α_0) is termed discontinuous precipitation (DP) [1–4]. In the event of a large interfacial energy of the α/β interfaces and/or substantial residual solute supersaturation (Δx) remaining in α following DP, a secondary reaction called discontinuous coarsening (DC) may replace the primary precipitation products with a similar two-phase aggregate having a distinctly coarser distribution/morphology [1, 4–6]. DC has also been reported to succeed eutectic [7], eutectoid [8] and similar moving boundary reactions (MBRs) during prolonged isothermal ageing [1]. Several theories have been proposed for the growth kinetics of DP [1–4, 9–15] and DC [4–8, 17]. In general, these models presume grain-boundary diffusion through the migrating boundary, called the reaction front (RF), to be the predominant mechanism of solute transport in DP/DC. Regarding the driving force for RF migration in DP, both chemical as well as interfacial free energy changes are known to have significant influences on the transformation kinetics [9–15]. On the other hand, an earlier model by Livingston and Cahn [8] assumes that the driving force for DC is derived solely from the

difference in interfacial free energies between the primary and secondary reaction products. However, it is known that solute content in the α -phase is unlikely to reach the equilibrium solvus immediately following DP [12, 16]. Accordingly, Fournelle [17] has extended an earlier growth kinetic model on DP by Petermann and Hornbogen [10] to DC, incorporating the supplementary contribution of the chemical driving force due to the Δx left in α following DP. This modified Petermann and Hornbogen model [17] is reported to yield a better estimate of the DC growth kinetics and Arrhenius parameters of boundary diffusivity in a number of systems like Fe–Ni–Ti [17], Al–Zn [6, 18], Ni–In [19, 20], Ni–Sn [21], Cu–Cd [22], and Fe–Zn [23].

DC in Zn–4 at % Ag alloy has recently been reported for the first time by Manna *et al.* [24]. However, the DC reaction reported in this study results from isothermal ageing at a higher or lower temperature than that for the preceding DP reaction, and hence is termed type II DC. The present paper presents a detailed study of the kinetics of DP as well as DCI (i.e. DP and DC at the same temperature) reactions in the same alloy for the first time. In addition, the Arrhenius parameters of diffusion of Ag in Zn–Ag have also been estimated using the relevant growth kinetic models for DP [9–12] and DC [17], and compared with the Arrhenius parameters

for grain-boundary self-diffusion of Zn [25] and volume diffusion of Ag in Zn [26] with the objective of determining the solute transport mode in DP/DCI in the present alloy.

2. Experimental procedure

The Zn–4 at % Ag alloy was prepared from high purity metals by vacuum-induction melting and casting (*in situ*) in an alumina crucible. The 8 mm diameter cylindrical cast ingot was homogenized at 683 K for two weeks under vacuum and quenched in water. Several discs of 5 mm thickness were cut from the ingot, solution annealed at 683 K for 14 h and quenched in water at room temperature. For DP and DCI studies, the solution-annealed samples were held isothermally in the temperature (T) range 353–573 K for different lengths of time (t) either in an oil bath (± 0.5 K) or in a muffle furnace (± 1 K) (with samples in evacuated glass capsules). DCI follows DP at the same temperature beyond a certain time. Samples for metallographic studies were prepared by mechanical polishing, and etching with a solution of 1 ml HNO_3 and 1 ml CH_3COOH in 98 ml of distilled water. While an optical microscope (OM) was utilized to determine the growth rate of the DP and DCI colonies and the repeat distance of the β phase, a detailed microstructural investigation by scanning electron microscopy (SEM) was carried out to study the growth morphology and mechanism of DP and DCI under different conditions. The average of the maximum normal distance between the original position of the boundary and its leading edge measured from 30–50 different colonies was calculated to represent the average maximum colony width (\bar{w}). It may be noted that the probable error in determining the true colony width (w) due to the difference in orientation of the DP and DCI colonies with respect to the plane of observation was corrected by multiplying \bar{w} by $\pi/4$ [27]. A similar correction was also applied to determine the true interlamellar spacing in a DP (λ_{DP}) or DCI (λ_{DCI}) colony by multiplying the average of the 20–30 independent measurements of such spacings obtained from the same microstructure.

In order to determine the average Ag concentration in α following DP and DCI, the lattice parameter of α at different temperatures was estimated by X-ray diffraction (XRD) analysis through peak-shift measurement of the $(1\ 1\ \bar{2}\ 0)_\alpha$ reflection, using $\text{CuK}\alpha$ (0.154 nm) radiation with a Ni filter and, adopting the necessary corrections for the systematic instrumental error. The lattice parameter was subsequently converted to the corresponding solute content using the appropriate lattice parameter–composition data reported in the literature [28].

3. Results and discussion

3.1. Mechanism of DP and DCI

Fig. 1 shows an SEM micrograph revealing the lamellar morphology of the β -phase interspaced within the α matrix in a DP colony formed at 433 K after 2 h. The constancy of λ_{DP} within a DP colony during the isother-

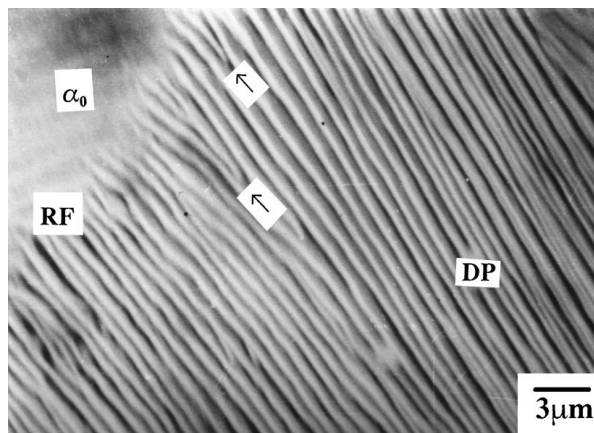


Figure 1 A typical DP colony formed at 433 K after 2 h. The arrowheads illustrate a possible mechanism of maintaining constancy of λ_{DP} (at a given T) by branching of the β -lamellae.

mal growth is ensured either by branching (Fig. 1) or by repeated nucleation of β on the migrating RF [2]. Careful study of the precipitate nucleation stage reveals that DP may be initiated either from one or from both sides of the same grain boundary separating two adjacent α_0 grains. However, all the grain boundaries are not equally potent in initiating DP, which may be attributed to the ability or otherwise of the boundary concerned to undergo thermally activated migration at the relevant temperature [29]. At a given temperature, the volume fraction of the DP colonies in the microstructure increases with an increase in time. However, DP is not the sole decomposition route for α_0 . At a higher temperature (say, at $T > 393$ K), the migrating RFs fail to consume the entire volume of all the α_0 grains. As a result, solute supersaturation in these untransformed α_0 grains above 393 K is relieved both by DP as well as concurrent continuous precipitation of Widmanstätten β , especially beyond a certain time (Fig. 2). In this regard, it is relevant to point out that precipitation in this alloy occurs entirely by the continuous/matrix mode in the range $T_{\text{DP}} < T < T_{\text{SV}}$, where T_{DP} is the highest temperature above which DP ceases and T_{SV} is the solvus temperature of the present alloy. From earlier studies,

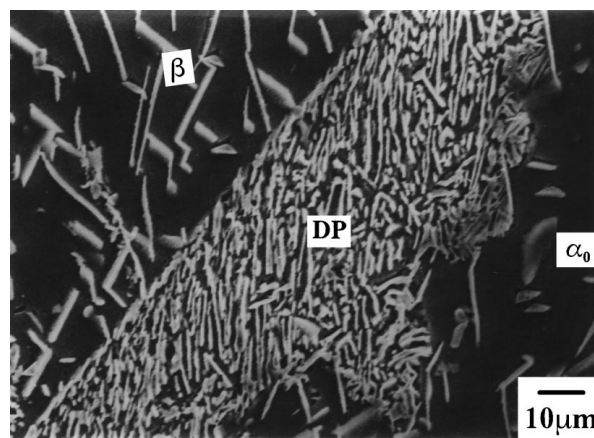
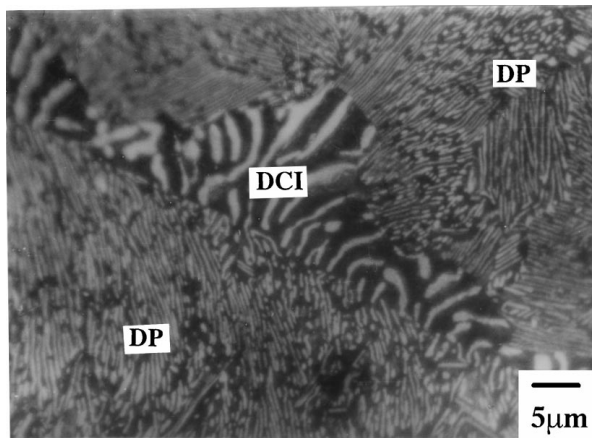
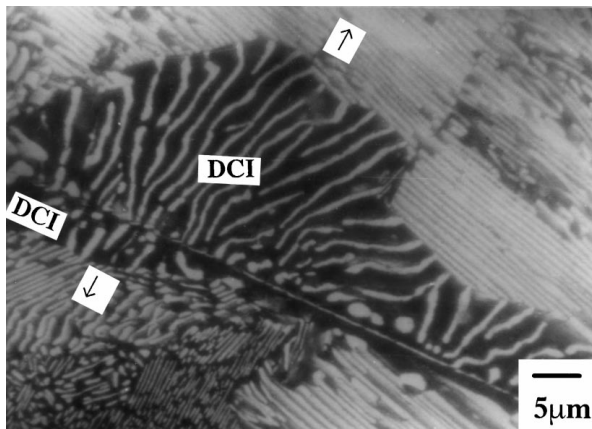


Figure 2 Formation of Widmanstätten β in the α_0 -matrix by continuous/matrix precipitation as a parallel mode of decomposition of α_0 along with DP at $T = 433$ K, $t = 4$ h.



(a)



(b)

Figure 3 (a) Growth of a DCI colony from the interfaces between two adjacent DP colonies at $T = 433$ K, $t = 50$ h (Note that the β -lamellae in the DCI and DP colonies are aligned parallel to each other); and (b) Growth of a DCI colony in opposite directions (shown by arrow-heads) from the same site of initiation, i.e. the interface between two DP colonies at $T = 433$ K, $t = 60$ h. (Note that: (i) the extent of growth in the upper DCI colony is more than that in Fig. 3a, (ii) the orientation relation between the β -lamellae in the DCI and DP colonies across the RF are opposite (perpendicular in the upper and parallel in the bottom colony), and (iii) the common site of initiation for both the DCI colonies has a greater than usual boundary width (see text).)

$T_{DP} = 621$ K [24] and $T_{SV} = 638$ K [28]. It may be pointed out that the very technique of determining T_{DP} ensures that T_{DP} is independent of the occurrence or otherwise of continuous precipitation.

In the course of isothermal precipitation for an extended period of t (when 70–90% of the α_0 grains have undergone DP), DCI replaces the primary reaction products of DP with a coarser distribution of the β lamellae. Fig. 3a shows the initiation of DCI from the boundary between two former DP colonies. A DCI colony gradually consumes the entire DP colony with a slower kinetics than that of the primary reaction. Fig. 3b shows the extent of growth of a DCI colony in the same sample after resuming the ageing for an additional time of 10 h at the same temperature. It may be noted that the extent of growth (w') for a longer time (Fig. 3b) is obviously greater than that for a shorter time (Fig. 3a). Fig. 3b further shows that another smaller DCI colony has been initiated and grown from the same interface with an opposite growth direction and a distinctly smaller w' under identical

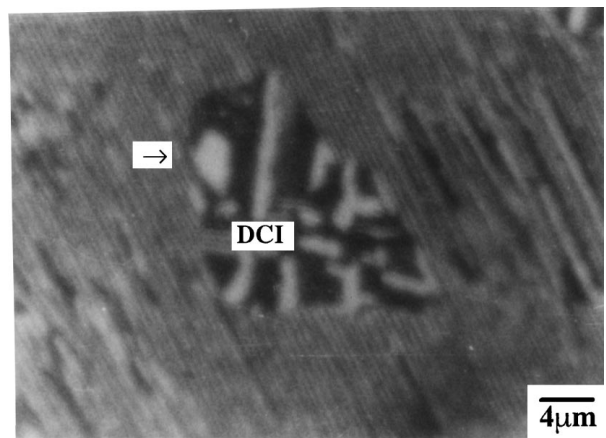


Figure 4 Initiation of an isolated DCI colony at the intersection between a former DP colony with the free (external) surface (indicated by an arrow-head).

ageing conditions. This difference may be attributed to the structural dependence of the mobility of a given RF in a typical MBR like DCI or DP [2, 29]. It is interesting to note that the common initiation site for the two DCI colonies in Fig. 3b (i.e. the interface between two former DP colonies) is characterized by a relatively greater than usual boundary width (i.e. 0.5 nm). The α/α_0 segments at the rear end of a DP colony are likely to be coherent/semi-coherent with the α_0/α grain trailing behind the original grain boundary (OGB) having a relatively poor mobility. Thus, it is difficult to conceive the initiation of two MBRs (i.e. DP followed by DCI) from the same interface either simultaneously or otherwise. However, the event shown in Fig. 3b seems to be similar to an earlier reported mechanism of DP initiation from a similar α/α_0 segment by converting the latter into a precipitate–matrix-type incoherent phase boundary due to precipitation of a solute-rich film on that segment [29].

In addition to grain/phase boundaries, a DCI reaction has also been observed to be initiated from the free surfaces intersecting a DP colony (Fig. 4) or from the DP-RFs. Incidentally, Fournelle [5] has also reported initiation of DCI from the DP-RFs in the Al–Zn alloys. However, Livingston and Cahn [8] have earlier predicted that DCI initiated at the junction of the two DP colonies would maintain a strict orientation relationship between the products of the primary and secondary colonies such that the colony having the lamellae parallel to the DC–RF would grow at the expense of that aligned perpendicular to the latter. However, the β -lamellae in the DCI colony are oriented parallel to those in the DP colony being consumed in Fig. 3a, but perpendicular to those in the primary colony ahead in Fig. 3b, respectively. Thus, Fig. 3a and b demonstrate that the Livingston and Cahn [8] orientation relationship between the primary and secondary reaction products is not mandatory in the present alloy. Possibly, the physical orientation relationship predicted by Livingston and Cahn [8] is applicable only when the precipitate and matrix phases maintain a strict crystallographic habit relationship between them for nucleation and cooperative growth. However, such an investigation is beyond the scope of the present work.

TABLE I Kinetic data on DP and DCI in Zn-4 at % Ag alloy

T (K)	v_{DP} ($m\ s^{-1}$)	λ_{DP} (μm)	v_{DCI} ($m\ s^{-1}$)	λ_{DCI} (μm)	$\lambda_{DCI}/\lambda_{DP}$
353	4.5×10^{-10}	0.44	3.9×10^{-12}	1.90	4.3
373	1.3×10^{-9}	0.45	8.3×10^{-12}	1.94	4.3
393	2.7×10^{-9}	0.45	1.5×10^{-11}	1.78	4.0
413	5.3×10^{-9}	0.49	5.2×10^{-11}	1.98	4.0
433	8.6×10^{-9}	0.50	7.2×10^{-11}	1.71	3.4
453	1.2×10^{-8}	0.55	1.5×10^{-10}	2.51	4.6
513	2.3×10^{-8}	0.82	—	—	—
573	1.4×10^{-8}	1.73	—	—	—

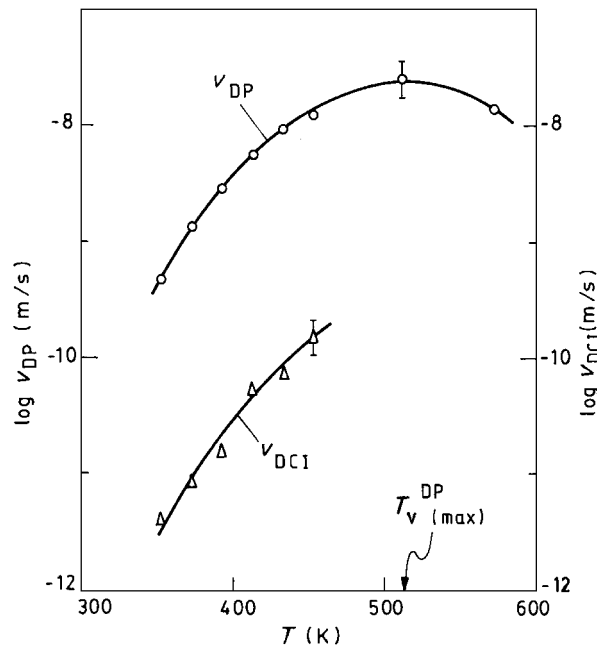


Figure 5 Variation of the RF migration velocity during DP (v_{DP}) and DCI (v_{DCI}) as a function of isothermal ageing temperature (T). $T_{v(max)}^{DP} = 513$ K corresponds to v_{max} (see text).

3.2. RF migration rate

The slope of the straight lines fitted to the data for the isothermal variation of w as a function of time represents the RF migration rate, either during DP (v_{DP}) or DCI (v_{DCI}), as the case may be. Table I presents the v_{DP} and v_{DCI} values at different temperatures. The variation of v_{DP} as a function of temperature exhibits a “C-curve” behavior with $v_{DP(max)}$ at $T = T_{v(max)}^{DP} = 513$ K (Fig. 5). It may be noted that $T_{v(max)}^{DP} = 0.81 T_{SV}$ in the present alloy, which is in fair agreement with an earlier prediction that the maximum growth rate in DP occurs at $(0.89 \pm 0.04)T_{SV}$ [30]. Interestingly, v_{DP} in the present alloy is always higher than that for another Zn–Ag alloy with lower (2 at % Ag) solute content at all comparable temperatures [31]. Thus, the chemical driving force has a significant influence on v_{DP} under comparable conditions of growth.

On the other hand, v_{DCI} exhibits a monotonic increase with an increase in temperature (Fig. 5). In contrast to the nature of the variation of v_{DP} with temperature, the absence of inversion of v_{DCI} with an increase in temperature in Fig. 5 (in the temperature range studied) may possibly arise due to the presence of a substantial

Δx and its supplementary (instead of decreasing) contribution to the chemical and overall driving force for DCI at higher temperatures of growth. It may be noted that determination of v_{DCI} at temperatures higher than those reported in Fig. 5 has not been feasible, mainly due to the fact that precipitation/coarsening by the continuous/matrix mode seems to prevail over that by the discontinuous mode at a higher temperature. However, v_{DCI} has always been lower by orders of magnitude than v_{DP} under the comparable conditions. This observation is consistent with the relevant data reported for other alloy systems [20–23]. In general, the slower growth rate in DCI may be attributed to the relatively smaller driving force for DCI than that for DP at a given temperature [17].

3.3. The interlamellar spacing

Both in DP as well as DCI, the β phase maintains a statistically constant distance of separation under steady-state growth conditions. Fig. 6 shows the variation of λ_{DP} and λ_{DCI} as a function of temperature for the present alloy. λ_{DP} increases monotonically as the temperature increases. However, a similar systematic variation of λ_{DCI} with temperature has not been recorded. Shaarbaf and Fournelle [18] have reported a similar non-systematic variation of λ_{DCI} with temperature in an Al–29.5 at % Zn alloy. However, a proper explanation for the non-systematic variation of λ_{DCI} in the present alloy is not possible at this stage.

Table I summarizes the experimentally determined kinetic data on DP and DCI. It may be noted that the coarsening ratio ($\lambda_{DP}/\lambda_{DCI}$) varies between 3 and 5 for the present alloy in the temperature range studied. This ratio has been reported to vary from as low as 1.8 for DC in a Ni–8.5 at % Sn alloy [21] to as high as 20 for the lamellar Ni–In eutectoid alloy [8]. Nevertheless, the values recorded in Table I compare well with the similar data of $\lambda_{DCI}/\lambda_{DP} = 4$ –8, reported earlier for an Al–29 at % Zn alloy [6].

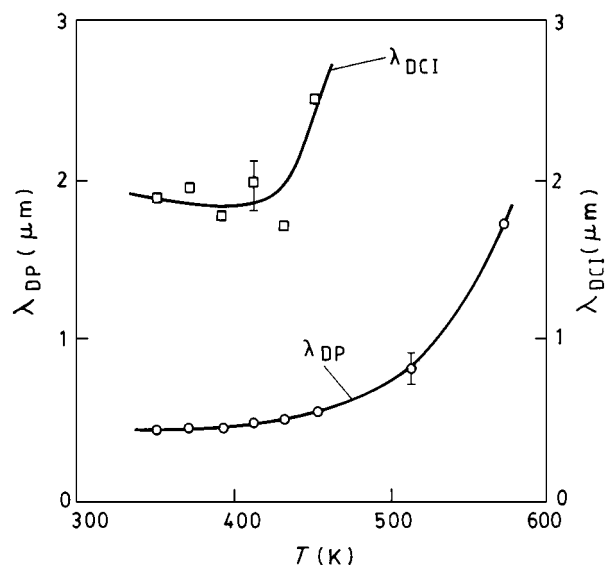
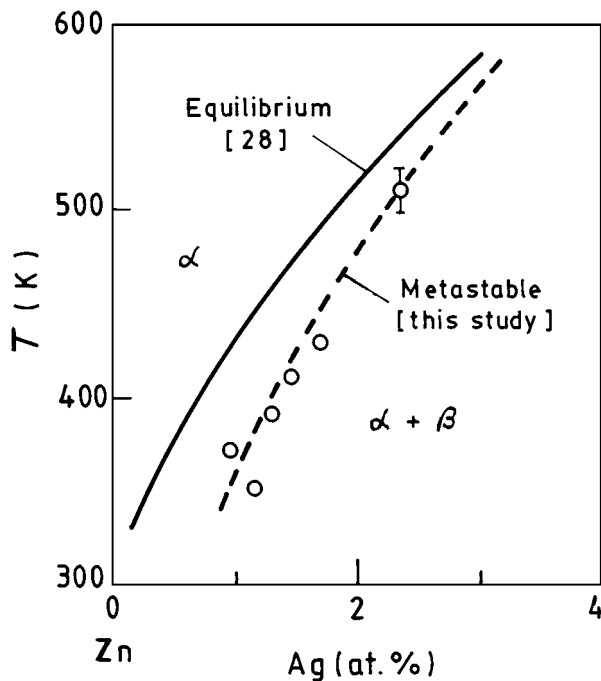


Figure 6 Variation of interlamellar spacing in DP (λ_{DP}) and DCI (λ_{DCI}) versus isothermal ageing temperature (T).

TABLE II Thermodynamic data for calculation of the driving force for DP (ΔG_{DP}) as a function of T for Zn-4 at % Ag alloy

T (K)	x_α^e (at %)	x_β^e (at %)	Ω	x_α^m (at %)	$-\Delta G_\beta$ (J mol ⁻¹)	$-\Delta G_\alpha^m$ (J mol ⁻¹)	$-\Delta G_\alpha^o$ (J mol ⁻¹)	$-\Delta G_{\alpha+\beta}^m$ (J mol ⁻¹)	$-\Delta G_{DP}^c$ (J mol ⁻¹)	γ (mJ m ⁻²)	ΔG_{DP}^γ (J mol ⁻¹)	$-\Delta G_{DP}$ (J mol ⁻¹)
353	0.30	12.6	2.7949	1.16	3177.9	279.1	806.5	998.8	192.3	292	12.1	180.2
373	0.45	12.6	2.9413	0.98	3257.3	258.9	869.6	1038.2	168.6	290	11.7	156.9
393	0.65	12.6	3.0763	1.31	3336.7	357.4	933.1	1067.3	134.2	288	11.6	122.5
413	0.85	12.6	3.1338	1.49	3416.1	423.2	988.2	1099.4	111.2	286	10.6	100.6
433	1.05	12.6	3.1531	1.70	3495.5	498.9	1038.7	1131.2	92.5	284	10.3	82.2
453	1.25	12.6	3.1516	1.80	3574.9	548.4	1086.5	1164.9	78.4	282	9.3	69.6
513	2.00	12.5	3.2297	2.38	3813.1	792.7	1233.7	1276.2	42.5	276	6.1	36.4
573	2.85	12.4	3.2727	3.00	4051.3	1078.4	1376.2	1394.7	18.5	270	2.8	15.7


 Figure 7 Metastable solvus curve for the Zn-Ag system indicating the average solute concentration (x_α^m) in the Zn-rich α phase following DP at a given T . The equilibrium solvus line [28] is shown here for comparison.

3.4. Average composition of the α phase

Cahn [12] predicted that the average solute content of the α -lamellae does not reach the equilibrium value (x_α^e) and follows a parabolic solute distribution profile (in α) between the β -lamellae immediately following DP. In other words, α is in metastable equilibrium with β following DP [16] and, may attain true equilibrium either by continuous/matrix precipitation or by DCI in the course of continued ageing, provided long-range solute transport is permissible. The metastable composition of α following DP in this study (x_α^m) (determined from XRD analysis) and x_α^e values are presented in Table II. Fig. 7 presents the equilibrium and metastable solvus curves for the Zn-Ag system to illustrate the extent of Δx remaining in the α phase following DP at a given temperature. It may be pointed out that the numerical difference between x_α^m and x_α^e is very small (Fig. 7). Hence, Δx following DCI, if at all present, may have negligible influence in the computation of the chemical driving force for DCI (ΔG_{DCI}^c) assuming the composition in α following DCI corresponds to x_α^e .

3.5. Analyses of DP (primary reaction) growth kinetics

Since the analytical treatment of the growth kinetics of eutectoid decomposition by Zener [32], a number of mathematical models have been proposed to analyze the kinetics of MBRs like DP and DC [7–15, 17]. In general, the models for DP correlate the intrinsic grain boundary diffusivity (D_b) with v_{DP} and λ_{DP} as follows

$$s\delta D_b = kv_{DP}\lambda_{DP}^2 \quad (1)$$

where s is the segregation factor [33], δ represents the grain boundary width and k is a function related to the solute partitioning between the α and β phases following DP. The function k assumes different expressions for different models. Kinetic analyses of DP in the present study have been confined to utilizing the more commonly applied models of Turnbull [9], Petermann and Hornbogen [10], Hillert [11] and Cahn [12].

The parameter k in Equation 1 in Turnbull's model [9] for DP is denoted as follows

$$k = x_\alpha^o / (x_\alpha^o - x_\alpha^m) \quad (2)$$

where x_α^o is the initial composition of the alloy. The parameter k in the Petermann and Hornbogen model [10] is expressed as follows

$$k = RT / (-8\Delta G_{DP}) \quad (3)$$

where R is the gas constant and ΔG_{DP} represents the overall change in Gibbs free energy in DP. Assuming negligible contribution of change in strain-free energy, ΔG_{DP} may be written as follows

$$\Delta G_{DP} = \Delta G_{DP}^c + \Delta G_{DP}^\gamma \quad (4)$$

where ΔG_{DP}^c and ΔG_{DP}^γ express the chemical and interfacial components of ΔG_{DP} , respectively. Now, the free energy (chemical) of formation of a solid solution, e.g. that of the α phase (ΔG_α^c), may be calculated by the regular solution model [34] as follows:

$$\Delta G_\alpha^c = RT[x_\alpha \ln x_\alpha + (1-x_\alpha) \ln(1-x_\alpha)] + \Omega RT x_\alpha(1-x_\alpha) \quad (5)$$

where x_α is the solute content in the β phase and Ω is a coefficient characteristic of the particular system at a given temperature [34]. It may be pointed out that x_α

may assume the values of x_α^o , x_α^m , or x_α^e , as and when the α phase exists in the form of a supersaturated, solute-depleted (metastable) phase or a solute-depleted (equilibrium) phase, respectively. The required value of Ω for this study is not available in the literature. Chaung *et al.* [19] have indirectly estimated the value of Ω through the following analytical expression

$$\Omega = \frac{(\Delta G_\beta/RT) - [x_\beta^e \ln x_\alpha^e + (1 - x_\beta^e) \ln(1 - x_\alpha^e)]}{(x_\alpha^e)^2 + x_\beta^e - 2x_\alpha^e x_\beta^e} \quad (6)$$

where x_β^e represents the equilibrium solute content in the β phase and ΔG_β refers to the Gibbs free energy of formation of the β phase. The estimated value of Ω at the corresponding temperature may be determined through Equation 6 subject to the availability of ΔG_β as a function of temperature. ΔG_β in the required composition and temperature range is not available in the literature. Hultgren *et al.* [35] have reported the enthalpy (ΔH_β) and entropy (ΔS_β) changes for the formation of the β phase for a limited range of composition only at $T = 873$ K. Extrapolating the values of ΔH_β and ΔS_β to $x_\beta^e = 0.126$ (Fig. 8) and assuming them to be temperature-independent, ΔG_β may now be calculated for the required range of temperature. Furthermore, the values of Ω , and consequently, ΔG_α may be estimated as a function of temperature through Equations 6 and 5, respectively (Table II).

Analytically, ΔG_{DP}^c may now be calculated as follows

$$\Delta G_{DP}^c = \Delta G_{\alpha+\beta}^m - \Delta G_\alpha^o \quad (7)$$

where $\Delta G_{\alpha+\beta}^m$ and ΔG_α^o refer to the free energy changes associated with the phase-mixture of α and β (following DP) and the standard free energy of formation for the α_o phase ($x_o = 0.04$), respectively. $\Delta G_{\alpha+\beta}^m$ may be

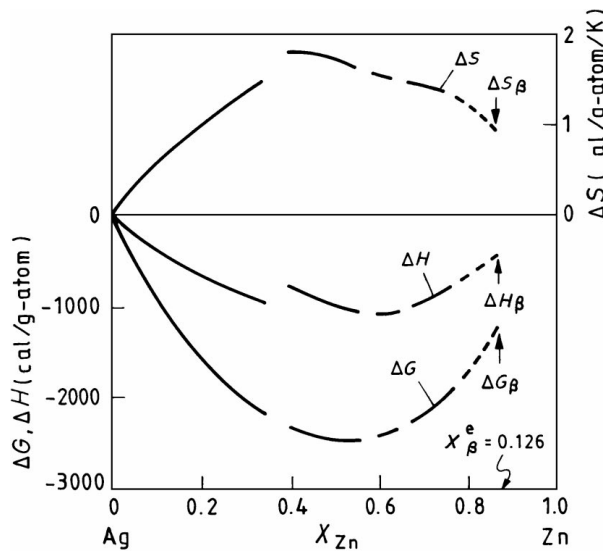


Figure 8 Determination of the free energy of formation of the β phase (ΔG_β) at the required composition of $x_\beta^e = 0.126$ by suitable extrapolation of the changes in enthalpy (ΔH_β) and entropy (ΔS_β) data reported by Hultgren *et al.* [35] for $T = 873$ K.

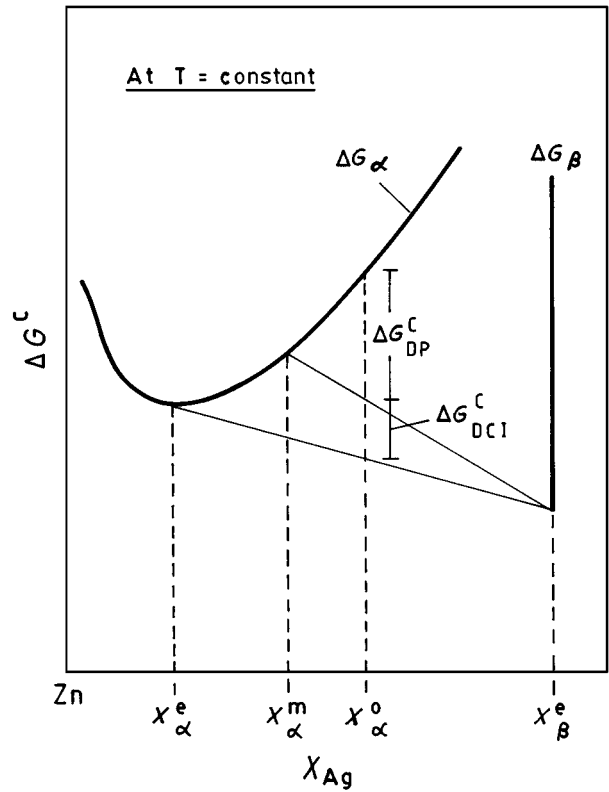


Figure 9 Schematic diagram illustrating the principle of determination of the available chemical driving force for DP (ΔG_{DP}^c) and DCI (ΔG_{DCI}^c) from the chemical free-energy change (ΔG^c) versus composition (x_{Ag}) diagram for the Zn-Ag system.

calculated from the respective values of ΔG_α and ΔG_β using the lever rule through the following expression

$$\Delta G_{\alpha+\beta}^m = [(x_\beta^e - x_\alpha^o)/(x_\beta^e - x_\alpha^m)] \Delta G_\alpha^m + [(x_\alpha^o - x_\alpha^m)/(x_\beta^e - x_\alpha^m)] \Delta G_\beta \quad (8)$$

ΔG_{DP}^c may now be computed using the values of $\Delta G_{\alpha+\beta}^m$ (through Equation 8) and ΔG_α^o (through Equation 5) at a given temperature. Fig. 9 schematically illustrates this procedure at a given temperature. Assuming a uniform stacking of β lamellae in the α matrix within the DP colony, ΔG_{DP}^γ may be expressed as follows [36]

$$\Delta G_{DP}^\gamma = 2 V_m \gamma / \lambda_{DP} \quad (9)$$

where V_m and γ represent the molar volume and specific energy of the α/β interfaces, respectively. Since γ for the Zn-Ag system is not available in the literature and the grain-boundary specific energy of pure Zn is 340 mJ m^{-2} at 573 K [37], it may be reasonable to assume that $\gamma = 270 \text{ mJ m}^{-2}$ at 573 K with $d\gamma/dT = -0.1 \text{ mJ m}^{-2} \text{ K}^{-1}$ for the Zn-4 at % Ag alloy. V_m for the ($\alpha + \beta$) aggregate in the present alloy has been calculated (by the rule of mixtures) to be $9.10 \times 10^{-6} \text{ m}^3 \text{ mol}^{-1}$. Thus, ΔG_{DP} may be calculated at a given temperature through Equation 4, incorporating the contributions of ΔG_{DP}^c and ΔG_{DP}^γ as per Equations 7 and 9, respectively. Table II summarizes the relevant thermodynamic data for calculating

TABLE III Calculated values of the parameter k and grain boundary chemical diffusivity triple product ($s\delta D_b$) from the models for DP by Turnbull [9], Petermann and Hornbogen [10], Hillert [11] and Cahn [12], respectively

T (K)	k				$s\delta D_b$ ($\text{m}^3 \text{s}^{-1}$)			
	[9]	[10]	[11]	[12]	[9]	[10]	[11]	[12]
353	1.41	2.03	0.21	0.26	1.2×10^{-22}	1.8×10^{-22}	1.8×10^{-23}	2.3×10^{-23}
373	1.32	2.47	0.35	0.46	3.5×10^{-22}	6.5×10^{-22}	9.2×10^{-23}	1.2×10^{-22}
393	1.49	3.33	0.26	0.32	8.2×10^{-22}	1.8×10^{-21}	1.4×10^{-22}	1.8×10^{-22}
413	1.59	4.26	0.25	0.32	2.0×10^{-21}	5.4×10^{-21}	3.2×10^{-22}	4.0×10^{-22}
433	1.74	5.46	0.23	0.28	3.7×10^{-21}	1.2×10^{-20}	5.0×10^{-22}	6.0×10^{-22}
453	1.82	6.75	0.27	0.32	6.8×10^{-21}	2.5×10^{-20}	1.0×10^{-21}	1.2×10^{-21}
513	2.47	14.62	0.30	0.34	3.8×10^{-20}	2.3×10^{-19}	4.7×10^{-21}	5.3×10^{-21}
573	4.00	37.86	0.49	0.54	1.6×10^{-19}	1.6×10^{-18}	2.0×10^{-20}	2.2×10^{-20}

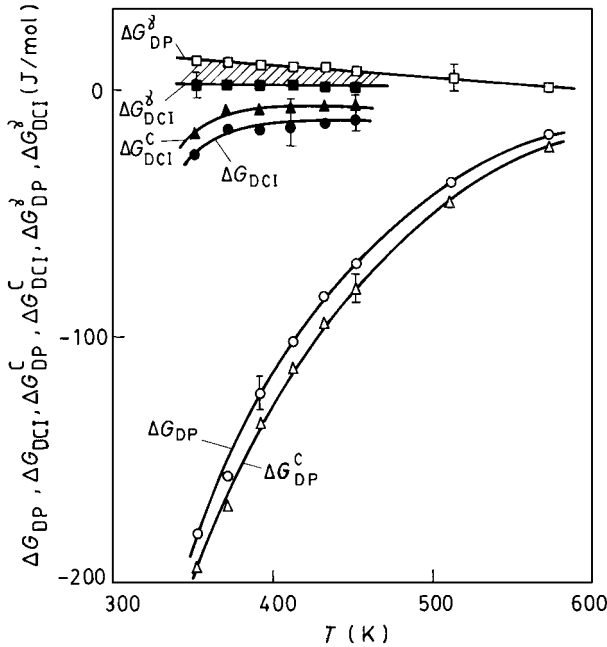


Figure 10 Variation of the overall driving force for DP and DCI along with their constituent components in terms of the respective Gibbs free-energy changes as a function of the isothermal ageing temperature (T).

ΔG_{DP} . Fig. 10 shows the variation of ΔG_{DP} , ΔG_{DP}^{γ} and ΔG_{DP}^C as a function of temperature. Finally, the estimated value of ΔG_{DP} may enable determination of the parameter k in Equation 3 and subsequently, $s\delta D_b$ as per the Petermann and Hornbogen model on DP [10] through Equation 1.

According to the Hillert model on DP [11], the value of the parameter k in Equation 1 is given by the following expression

$$k = \lambda_{DP}^{\alpha} (x_{\alpha}^o - x_{\alpha}) / [12 \lambda_{DP} (x_{\alpha} - x_{\alpha/\beta})] \quad (10)$$

where λ_{DP}^{α} refers to the width of the α lamellae, x_{α} denotes the variable composition of the α phase as a function of the lateral distance between the β lamellae, and $x_{\alpha/\beta} = x_{\alpha}$ at the α/β interface. Avoiding Hillert's proposed method of calculating x_{α} and $x_{\alpha/\beta}$ analytically for the lack of the relevant data in the present case and assuming $x_{\alpha/\beta} = x_{\alpha}^e$ and $x_{\alpha} = x_{\alpha}^m$, the modified value of k may be found as follows

$$k = \lambda_{DP}^{\alpha} (x_{\alpha}^o - x_{\alpha}^m) / [12 \lambda_{DP} (x_{\alpha}^m - x_{\alpha}^e)] \quad (11)$$

The value of k in Equation 1 after Cahn's theory for DP [12] assumes the form

$$k = 1/C \quad (12)$$

where C is the Cahn parameter related to the fraction of solute supersaturation consumed in DP, and is given by

$$(2/C^{1/2}) \tanh(C^{1/2}/2) = (x_{\alpha}^o - x_{\alpha}^m) / (x_{\alpha}^o - x_{\alpha}^e) \quad (13)$$

The calculated values of k for the different models for DP are presented in Table III.

From the experimentally determined values of v_{DP} , λ_{DP} and x_{α}^m , $s\delta D_b$ may be calculated as a function of temperature through the four models expressed by the general Equation 1 after incorporating the respective value of k . Table III summarizes the $s\delta D_b$ values calculated using these models in the range $T = 353$ – 573 K.

3.6. Analysis of DCI (secondary reaction) growth kinetics

DCI involves substitution of the fine lamellar products of DP with a similar two-phase aggregate having a distinctly coarser distribution during extended isothermal ageing at a given temperature. The Livingston and Cahn model [8] assumes that the driving force for the secondary reaction is derived solely from the reduction in interfacial area/energy as $\Delta x = (x_{\alpha}^m - x_{\alpha}^e) = 0$ following DP. However, XRD analysis in the present investigation has shown that the solute content in the α phase following DP is $x_{\alpha}^m (> x_{\alpha}^e)$, which subsequently reaches x_{α}^e after DCI (cf. Fig. 7). Therefore, the overall driving force for DCI (ΔG_{DCI}) may be given by [17]

$$\begin{aligned} \Delta G_{DCI} &= (\Delta G_{\alpha+\beta}^e - \Delta G_{\alpha+\beta}^m) + (\Delta G_{DCI}^{\gamma} - \Delta G_{DP}^{\gamma}) \\ &= \Delta G_{DCI}^c + (\Delta G_{DCI}^{\gamma} - \Delta G_{DP}^{\gamma}) \end{aligned} \quad (14)$$

where $\Delta G_{\alpha+\beta}^e$ is the modified form of $\Delta G_{\alpha+\beta}^m$ in Equation 8 (obtained by substituting x_{α}^m with x_{α}^e) and, similarly, ΔG_{DCI}^{γ} (analogous to ΔG_{DP}^{γ}) is calculated by replacing λ_{DP} with λ_{DCI} in Equation 9, respectively. Table IV presents the summary of the relevant thermodynamic data necessary for the derivation of ΔG_{DCI} . The magnitude of ΔG_{DCI} with its constituent components in the range of temperature studied has been shown in Fig. 10.

TABLE IV Gibbs free energy change and $s\delta D_b$ (using Equation 15) values for DCI in Zn– 4 at % Ag alloy

T (K)	$-\Delta G_\alpha^e$ (J mol ⁻¹)	$-\Delta G_{\alpha+\beta}^e$ (J mol ⁻¹)	$-\Delta G_{\text{DCI}}^e$ (J mol ⁻¹)	ΔG_{DCI}^v (J mol ⁻¹)	$-\Delta G_{\text{DCI}}$ (J mol ⁻¹)	$s\delta D_b$ (m ³ s ⁻¹)
353	84.0	1014.7	15.9	2.8	25.2	8.0×10^{-22}
373	130.0	1043.7	5.5	2.7	14.5	8.3×10^{-22}
393	192.7	1074.1	6.8	2.9	15.5	1.2×10^{-21}
413	258.5	1105.0	5.6	2.6	13.6	6.4×10^{-21}
433	327.2	1136.4	5.2	3.0	12.5	7.5×10^{-21}
453	398.9	1168.4	3.5	2.0	10.8	4.0×10^{-20}

Fournelle [17] has modified the analytical model for DP by Petermann and Hornbogen [10] to extend the scope of its application to DCI in the following way.

$$s\delta D_b = RT v_{\text{DCI}} \lambda_{\text{DCI}}^2 / (-8\Delta G_{\text{DCI}}) \quad (15)$$

The experimental data for λ_{DCI} and v_{DCI} required for the determination of $s\delta D_b$ through Equation 15 are listed in Table I. Finally, Table IV presents the $s\delta D_b$ values determined from Equation 15.

3.7. Determination of Arrhenius parameters of boundary chemical diffusivity

The temperature dependence of $s\delta D_b$ is typically expressed through an Arrhenius type of equation as follows

$$s\delta D_b = (s\delta D_b)_o \exp(-Q_b/RT) \quad (16)$$

where $(s\delta D_b)_o$ is the pre-exponential constant and Q_b is the activation energy of boundary chemical diffusion. Fig. 11 shows the Arrhenius plot of $s\delta D_b$ derived using the different models on DP [9–12] and DCI [17]. A satisfactory straight-line fit to the respective set of data obtained by regression analysis allows determination of the Arrhenius parameter from each of the straight lines in Fig. 11. Table V summarizes the Arrhenius parameters obtained in the present study under different conditions and compares them with the relevant data reported in the literature. The values of Q_b determined by the models of Turnbull [9], Cahn [12] and Hillert [11] are quite close to each other. Similarly, Q_b obtained through the Petermann and Hornbogen model on DP

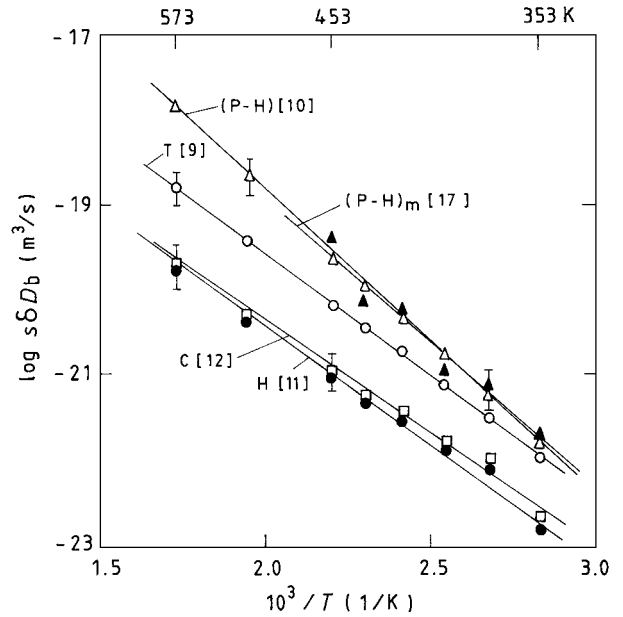


Figure 11 Arrhenius plot of grain-boundary chemical-diffusivity triple product ($s\delta D_b$) derived from various analytical models. Key: Turnbull [9], (T); Petermann–Hornbogen [10], (P-H); Hillert [11], (H); Cahn [12], (C); Petermann–Hornbogen, modified by Fournelle [17], (P-H)_m.

[10] and modified Petermann and Hornbogen model on DCI [17] compare well with each other, even though these values are relatively high compared to those derived by the other three models [9, 11, 12]. It has earlier been pointed out [36] that the $s\delta D_b$ values obtained by the Petermann and Hornbogen model on DP [10] are usually a few orders of magnitude higher than those obtained by the Cahn model [12]. However, the values of Q_b are comparable to the activation energy for grain-

TABLE V Arrhenius parameters of grain-boundary chemical diffusion determined through kinetic analysis of DP and DCI

Process	Model	$(s\delta D_b)_o$ (m ³ s ⁻¹)	Q_b (kJ mol ⁻¹)	Q_b/Q_v
DP	Turnbull [9]	1.3×10^{-14}	54.3	0.49
DP	Petermann–Hornbogen [10]	2.3×10^{-12}	68.2	0.61
DP	Petermann–Hornbogen (obtained from [24])	6.0×10^{-11}	65.8	0.59
DP	Hillert [11]	7.2×10^{-16}	50.5	0.45
DP	Cahn [12]	6.0×10^{-16}	49.1	0.44
DCI	Modified Petermann–Hornbogen [17]	2.8×10^{-12}	66.2	0.59
–	Grain boundary self-diffusion in Zn [25]	1.9×10^{-14}	61.1	0.55
–	Tracer impurity diffusion of Ag ¹¹⁰ in Zn [26]	$D_0 =$ 3.9×10^{-5} m ² s ⁻¹	$Q_v =$ 112.0	1.00

boundary self-diffusion in Zn [25], and nearly 50% of that for tracer diffusion (volume/matrix) of Ag¹¹⁰ in Zn (Q_v) [26].

It is relevant to point out that a certain amount of uncertainty in the Q_b values reported in Table V cannot be ruled out due to (a) the error (experimental) in determining v_{DP} , v_{DCI} , λ_{DP} and λ_{DCI} , (b) the error in estimating the overall driving force due to the necessary approximations, and (c) the inherent assumptions on which the analytical models used are based. However, the limit of cumulative uncertainty in Q_b in the present study would not exceed $\pm 10\%$, even by the most conservative estimate.

4. Summary and conclusions

1. α_0 in Zn-4 at % Ag alloy decomposes predominantly by DP at $T < 393$ K, and both by DP as well as continuous/matrix precipitation at $T \geq 393$ K during isothermal ageing in the range $T = 353$ – 573 K. Furthermore, DCI (secondary reaction) succeeds DP (primary reaction) in the course of continued isothermal ageing in the range 353–453 K.

2. DCI may be initiated from one of the following sites: junction of two DP colonies, edges of a DP colony (i.e. DP–RF), or intersection of a DP colony with the free (external) surface.

3. In DCI in Zn-4 at % Ag alloy, the precipitate lamellae do not maintain a rigid orientation-relationship, as predicted by Livingston and Cahn [8] between the precipitate phases in the parent (primary) and product (secondary) colonies.

4. The residual solute supersaturation remaining in α following DP provides an additional driving force for DCI.

5. Both λ_{DP} and λ_{DCI} increase with an increase in temperature, though the change of λ_{DCI} with temperature is not as systematic as that of λ_{DP} with temperature.

6. v_{DP} as a function of temperature displays a typical “C” curve variation with the maximum at 513 K. However, the same function for DCI increases monotonically in the temperature range studied.

7. DCI is characterized by $\lambda_{DCI} > \lambda_{DP}$ (by 3–5 times), and $v_{DCI} < v_{DP}$ (by 1–2 orders of magnitude) under comparable ageing conditions.

8. The activation energy values determined from the kinetic analyses of the DP and DCI reactions compare well with that for the boundary self-diffusion of Zn, and are about half that for the tracer volume diffusion of Ag in Zn. Thus, the DP and DCI reactions in the present alloy seem to be boundary diffusion-controlled processes.

9. The modified Petermann and Hornbogen model, proposed by Fournelle, seems more appropriate for kinetic analysis of DCI in the present alloy than that proposed by Livingston and Cahn [8].

Acknowledgements

The partial financial support from the Council of Scientific & Industrial Research (Grant No. 10/147/91/EMR-II) and the equipment support from the Board of

Research for Nuclear Sciences (Grant No. 34/7/89-G) are gratefully acknowledged.

References

1. R. D. DOHERTY, in “Physical Metallurgy,” edited by R. W. Cahn and P. Hansen (North-Holland Physics, Amsterdam, 1983) p. 996.
2. D. B. WILLIAMS and E. P. BUTLER, *Int. Met. Rev.* **26** (1981) 153.
3. W. GUST, in “Phase Transformation,” Series 3, No. 11, Vol. 1, edited by The Institution of Metallurgists (The Chameleon Press, London, 1979) p. II/27.
4. M. FRIESEL, I. MANNA and W. GUST, *Colloque Phys.* **51** (1990) C1–381.
5. R. A. FOURNELLE, *Acta Metall.* **27** (1979) 1135.
6. C. P. JU and R. A. FOURNELLE, *ibid.* **33** (1985) 71.
7. M. KAYA and R. W. SMITH, *ibid.* **37** (1989) 1657; **37** (1989) 1667.
8. J. D. LIVINGSTON and J. W. CAHN, *ibid.* **22** (1974) 495.
9. D. TURNBULL, *ibid.* **3** (1955) 55.
10. J. PETERMANN and E. HORNBOGEN, *Z. Met. kd.* **59** (1968) 824.
11. M. HILLERT, *Acta Metall.* **30**, 1689 (1982); *Metall. Trans. A* **3** (1972) 2729.
12. J. W. CAHN, *Acta Metall.* **7** (1959) 18.
13. B. E. SUNDQUIST, *Metall. Trans. A* **4** (1973) 1919.
14. J. M. SHAPIRO and J. S. KIRKALDY, *Acta Metall.* **16** (1968) 1239.
15. H. I. AARONSON and Y. C. LIU, *Scr. Metall.* **2** (1968) 1.
16. I. MANNA, J. SWAMINATHAN and S. K. PABI, *Z. Met. kd.* **85** (1994) 50.
17. R. A. FOURNELLE, *Acta Metall.* **27** (1979) 1147.
18. M. SHAARBAF and R. A. FOURNELLE, *Mater. Sci. Eng. A* **102** (1988) 271.
19. T. H. CHUANG, R. A. FOURNELLE, W. GUST and B. PREDEL, *Acta Metall.* **36** (1988) 775.
20. S. P. GUPTA and R. NAKKALIL, *ibid.* **38** (1990) 1871.
21. S. P. GUPTA, *ibid.* **35** (1987) 747.
22. S. P. GUPTA, *Z. Met. kd.* **77** (1986) 472.
23. T.-H. CHUANG, W. GUST, B. PREDEL and R. A. FOURNELLE, *Mater. Sci. Eng. A* **112** (1989) 175.
24. I. MANNA, J. N. JHA and S. K. PABI, *J. Mater. Sci.* **31** (1996) 2401.
25. E. S. WAJDA, *Acta Metall.* **2** (1954) 184 [cited by I. Kaur, W. Gust and L. Kozma, in “Handbook of Grain and Interphase Boundary Diffusion Data,” Vol. 2, (Ziegler Press, Stuttgart, 1989) p. 1416].
26. J. H. ROSOLOWSKI, *Phys. Rev.* **124** (1961) 1828 [cited by C. J. Smithells and E. A. Brandes, in “Metals Reference Book,” 5th edition (Butterworths, London, 1976) p. 881].
27. R. LÜCK, *Z. Met. kd.* **66** (1975) 448.
28. A. V. WIEDEBACH-NOSTIZ, *ibid.* **37** (1946) 56.
29. I. MANNA, S. K. PABI and W. GUST, *J. Mater. Sci.* **26** (1991) 4888; and *Acta Metall. Mater.* **39** (1991) 1489.
30. W. GUST, T. H. CHUANG and B. PREDEL, in “Decomposition of alloys: the early stages,” edited by P. HANSEN *et al.* (Pergamon Press, Oxford, 1984) p. 208.
31. I. MANNA, J. N. JHA and S. K. PABI, *Scr. Metall.* **29** (1993) 817.
32. C. ZENER, *Trans. AIME* **167** (1946) 550.
33. G. B. GIBBS, *Phys. Status Solidi* **16** (1966) K27.
34. R. A. SWALIN, in “Thermodynamics of Solids” (John Wiley & Sons, New York, 1962) p. 102.
35. R. HULTGREN, R. L. ORR, P. D. ANDERSON and K. K. KELLEY, in “Selected Values of Thermodynamic Properties of Metals and Alloys” (John Wiley & Sons, New York, 1963) p. 397.
36. I. KAUR and W. GUST, in “Fundamentals of Grain and Interphase Boundary Diffusion,” 2nd Edn. (Ziegler Press, Stuttgart, 1989) p. 232.
37. L. E. MURR, in “Interfacial Phenomena in Metals and Alloys” (Addison-Wesley, London, 1975) p. 133.

Received 20 October 1997

and accepted 19 August 1998